Acta Crystallographica Section D
Biological Crystallography
ISSN 0907-4449

Structure of human ferritin L chain

Zhongmin Wang, Chester Li, Melanie Ellenburg, Elizabeth Soistman, John Ruble, Brenda Wright, Joseph X. Ho and Daniel C. Carter*

New Century Pharmaceuticals Inc., 895 Martin Road, Huntsville, Alabama 35824, USA

Correspondence e-mail: dcarter@newcenturypharm.com

Received 13 March 2006
Accepted 17 May 2006

Ferritin is the major iron-storage protein present in all cells. It generally contains 24 subunits, with different ratios of heavy chain (H) to light chain (L), in the shape of a hollow sphere hosting up to 4500 ferric Fe atoms inside. H-rich ferritins catalyse the oxidation of iron(II), while L-rich ferritins promote the nucleation and storage of iron(III). Several X-ray structures have been determined, including those of L-chain ferritins from horse spleen (HoSF), recombinant L-chain ferritins from horse (HoLF), mouse (MoLF) and bullfrog (BfLF) as well as recombinant human H-chain ferritin (HuHF). Here, structures have been determined of two crystal forms of recombinant human L-chain ferritin (HuLF) obtained from native and perdeuterated proteins. The structures show a cluster of acidic residues at the ferrihydrite nucleation site and at the iron channel along the threefold axis. An ordered Cd^{2+} structure is observed within the iron channel, offering further insight into the route and mechanism of iron transport into the capsid. The loop between helices *D* and *E*, which is disordered in many other L-chain structures, is clearly visible in these two structures. The crystals generated from perdeuterated HuLF will be used for neutron diffraction studies.

1. Introduction

Iron, an essential nutrient in all living systems, is required for synthesis of the iron-porphyrin proteins, such as haemoglobin, myoglobin, cytochromes and cytochrome oxidase (Ford *et al.*, 1984; Theil, 1987). The iron molecules, which are insoluble in the native form under physiological conditions, are stored in all tissues as a ferrihydrite core enclosed by ferritin, a multimeric protein present in virtually all organisms. Ferritin plays an essential role in iron detoxification and acts as a large reservoir for iron in bioavailable form.

Ferritin is typically a 24-subunit spherical capsid with cubic 432 point symmetry, an outer diameter of ∼125 Å and an inner hollow core diameter of ∼80 Å (Ford *et al.*, 1984; Lawson *et al.*, 1991; Trikha *et al.*, 1995). Hydrophilic and hydrophobic pores penetrate the capsid at the eight threefold and six fourfold axes, respectively. It is largely accepted that iron enters the ferritin capsid *via* the pores located at the threefold axes and it is suggested that bimolecular oxygen, required for the oxidation of Fe^{2+}, enters through the hydrophobic pores at the fourfold axes. Each ferritin capsid has the capacity to store up to 4500 irons in the mineralized core. The ferritin monomer exists in several isoforms, which differ in their amino-acid sequences and molecular sizes. Two forms have been identified in human tissues, heavy chain (H chain; ∼21 kDa) and light chain (L chain; ∼19 kDa), with ratios

ranging from 2:22 to 20:4 (Harrison & Arosio, 1996). H-rich ferritins catalyse the oxidation of iron(II), while L-rich ferritins promote the nucleation and storage of iron(III). Isoferritins rich in H chain are associated with rapid iron uptake, serving a protective role in H-rich tissues such as the heart, brain and red blood cells, while L-rich ferritins have slower iron uptake but have larger mineralized cores and are primarily found in the liver, spleen or plasma. Generally, L-rich ferritins are more structurally stable against chemical and heat denaturation.

Several ferritin structures have been determined by other groups, including those of HuHF and HoLF (Ford *et al.*, 1984; Gallois *et al.*, 1997; Hempstead *et al.*, 1997; Lawson *et al.*, 1991; Trikha *et al.*, 1995). HuLF shares 87% sequence identity with the light-chain ferritin from horse, HoLF, but only 53% with its H-chain counterpart in humans, HuHF. Typically, there is a greater sequence homology between the same isoforms from different species than there is between the H and L chains within the same species. Despite highly conserved sequence with other L-chain ferritins, the HuLF structure has not been determined owing to a lack of diffraction-quality crystals (Hempstead *et al.*, 1997). Here, we describe the X-ray structures of recombinant HuLF from two forms of crystals grown from the native and perdeuterated proteins and compare for the first time the structures of H- and L-chain capsids from the same species.

2. Materials and methods

2.1. Protein expression and purification

The DNA coding for HuLF was cloned into pET-11a (Novagen, San Diego, CA. USA) through the restriction sites *Nde*I and *Bam*HI using a PCR-based method. The coding region of the resulting plasmid pET-11a-LF was verified by automated DNA sequencing. The construct was then transformed into BL21 (DE3) bacterial protein-expression cells. The positive transformant was grown in LB medium with ampicillin (100 mg ml^{-1}) overnight and subsequently diluted (1:50) into fresh LB medium containing ampicillin. The growth of the culture was monitored spectrophotometrically and 1.0 m*M* IPTG (isopropyl β-D-1-thiogalactopyranoside) was added to the culture to induce protein expression when the cell density reached an $A_{600\,\mathrm{nm}}$ of 0.6. The cells were collected after 3–5 h induction and were resuspended in B-PER buffer (Pierce, Rockford, IL, USA) to release the proteins. The cells were centrifuged at 27 500*g* for 30 min and the supernatant was transferred to a fresh tube for heat treatment (343 K for 10 min). The sample was then centrifuged to remove denatured protein. The supernatant containing HuLF was first applied onto a gel-filtration column (S-300), taking advantage of the large molecular size of the 24-mer capsid (~450 kDa), followed by ion-exchange (DEAE) chromatography. The eluted fractions were monitored at 280 nm and analysed by SDS–PAGE. The final protein was dialyzed in 50 m*M* Tris buffer pH 7.0 and stored at 277 K.

Perdeuterated HuLF was produced using the same procedure outlined above with the culture-medium components replaced with D_2O and deuterated material as far as possible. The purified protein was verified by mass spectrometry to be more than 90% perdeuterated. Detailed procedures and results for perdeuteration will be published elsewhere.

2.2. Crystallization and data collection

Prior to setting up crystallization, recombinant HuLF was extensively dialyzed against Nanopure water or D_2O for several days to remove buffering agent or to complete the proton exchange and then concentrated to around 10 mg ml^{-1}. Several crystal forms were produced from screening conditions ranging from low-molecular-weight PEGs to high concentrations of ammonium sulfate. Each form was individually examined for X-ray diffraction. All but two forms of crystals diffracted to very poor resolution, possibly owing to lattice disorder inside the crystals.

One form, identified as rhombohedral, space group *R*32, was grown by sitting-drop vapor diffusion, with 5 µl protein mixed with 5 µl reservoir solution containing 30% Jeffamine M-600, 0.05 *M* caesium chloride and 0.1 *M* sodium citrate buffer pH 5–6 in Cryschem plates (Charles Supper Co., Natick, MA, USA). The crystals were flash-frozen directly from the drop in liquid nitrogen and a data set (*R*32) was collected at the NSLS X12B station at Brookhaven National Laboratory (BNL) on a crystal grown from perdeuterated protein to 2.5 Å resolution, with unit-cell parameters $a = b = 183$, $c = 354$ Å, $\alpha = \beta = 90.0$, $\gamma = 120.0^\circ$ and eight ferritin monomers in the asymmetric unit.

Another crystal form belongs to the *I*-centered cubic space group *I*432, with unit-cell parameters $a = b = c = 152$ Å, $\alpha = \beta = \gamma = 90.0^\circ$. The crystals were grown by sitting-drop vapor diffusion, with 5 µl protein mixed with 5 µl reservoir solution consisting of 1.6% $CdSO_4$ in 0.2 *M* sodium acetate pH 5–6 in Cryschem plates. These crystals were frozen in liquid nitrogen with 20% ethylene glycol added to the mother liquor as a cryoprotectant. A data set to 1.9 Å resolution (lt-*I*432) was collected at NSLS X12B station at BNL on a crystal grown from perdeuterated protein. Another data set was collected at room temperature to 2.1 Å resolution (rt-*I*432) on an R-AXIS IV detector mounted on a Rigaku RU-H3R rotating-anode generator operated at 5.0 kW (50 kV, 100 mA). This crystal was grown from native protein. There is one monomer in the asymmetric unit.

The experimental results reported here utilized crystals from ground-based preparations in support of microgravity crystal-growth experiments performed on the International Space Station. Crystals from the microgravity experiments were returned on STS-114 in August 2005 after an unplanned unusually long 2.5 y growth period. Once completed, detailed analyses of these crystals will be reported separately.

2.3. Structure determination and refinement

Attempts to solve the *R*32 structure using monomer structures from HuHF and several L-chain ferritins of other species

as search models in molecular replacement were unsuccessful owing to the large number of potential solutions.

Careful inspections revealed that the *R*32 unit cell has a subclass of *C*2, defined by unit-cell parameters $a = 258.477$, $b = 182.614$, $c = 158.280$ Å, $\alpha = 90.0$, $\beta = 114.097$, $\gamma = 90.0^\circ$. Data reindexed in this unit cell enabled the asymmetric unit to contain the entire 24 subunits. Therefore, the hollow sphere of HuHF was reconstituted from the monomer structure using crystallographic symmetry and used as a search model. As expected, the solution in the *C*2 cell has its internal threefold axis coincident with the crystallographic threefold axis of the *R*32 cell. Upon finding the *C*2 solution, the conversion to *R*32 form was accomplished by choosing one-third of the 24 monomers inside the rhombohedral asymmetric unit. After simulated annealing and initial positional refinement, the amino acids were substituted with the HuLF sequence. Restrained non-crystallographic symmetry was employed throughout and was released at the end of refinement.

The *I*432 structures were solved by molecular replacement using a single molecule from the *R*32 form as the search model.

The refinements were carried out with *CNX* (Brünger *et al.*, 1998) and model adjustments were performed interactively in the program *CHAIN* (Sack & Quiocho, 1997). Water molecules were picked automatically and inspected graphically. Alternative side-chain conformations were modeled manually when both $(2F_o - F_c)$ and $(F_o - F_c)$ electron-density maps were clearly visible. Metal ions and other bound substances were identified and refined toward the end. The final models have good statistics and geometry (Table 1).

Table 1
Statistics from the crystallographic analysis.

Data set	*R*32 form (100 K)	lt-*I*432, 100 K	rt-*I*432 (293 K)
Protein	Perdeuterated	Perdeuterated	Native
Resolution range (Å)	50.0–2.5	50.0–1.9	30.0–2.1
Observed reflections	1989690	569448	206812
Unique reflections	79092	23698	18119
Data completeness (%)	91.6 (55.4)	100 (100)	96.1 (81.5)
Multiplicity	5.1 (2.2)	5.3 (4.9)	5.0 (4.3)
Intensities $[I/\sigma(I)]$	6.6	7.4	15.5
R_{sym}† (%)	13.8	10.0	10.2
Unit-cell parameters (Å, °)	$a = b = 182.79$, $c = 354.23$, $\alpha = \beta = 90.0$, $\gamma = 120.0$	$a = b = c = 151.60$, $\alpha = \beta = \gamma = 90.0$	$a = b = c = 152.87$, $\alpha = \beta = \gamma = 90.0$
R factor (%)	22.4	21.0	19.4
R_{free} (%)	26.7	24.0	22.0
No. of water atoms	147	156	99
No. of metal ions	10	14	13
Average *B* (Å^2)			
Main chain	43.41	20.34	20.05
Side chain	44.27	21.58	22.09
R.m.s.d. from ideality‡			
Bond lengths (Å)	0.008	0.005	0.005
Bond angles (°)	1.3	1.1	1.1
Dihedral angles (°)	19.8	18.6	18.3
Improper angles (°)	0.76	0.68	0.69
Ramachandran plot§ (%)			
Most favored regions	91.0	94.8	94.1
Allowed regions	8.3	5.2	5.9
Disallowed regions	0.6	0	0

† $R_{sym} = \sum I_j - \langle I_j \rangle / \sum \langle I_j \rangle$, where I_j is the intensity of an observation of reflection j and $\langle I_j \rangle$ is the average intensity for reflection j. ‡ The root-mean-square deviations (r.m.s.d.s) were calculated using the program *CNX* (Brünger *et al.*, 1998). § As checked with the program *PROCHECK* (Laskowski *et al.*, 1993).

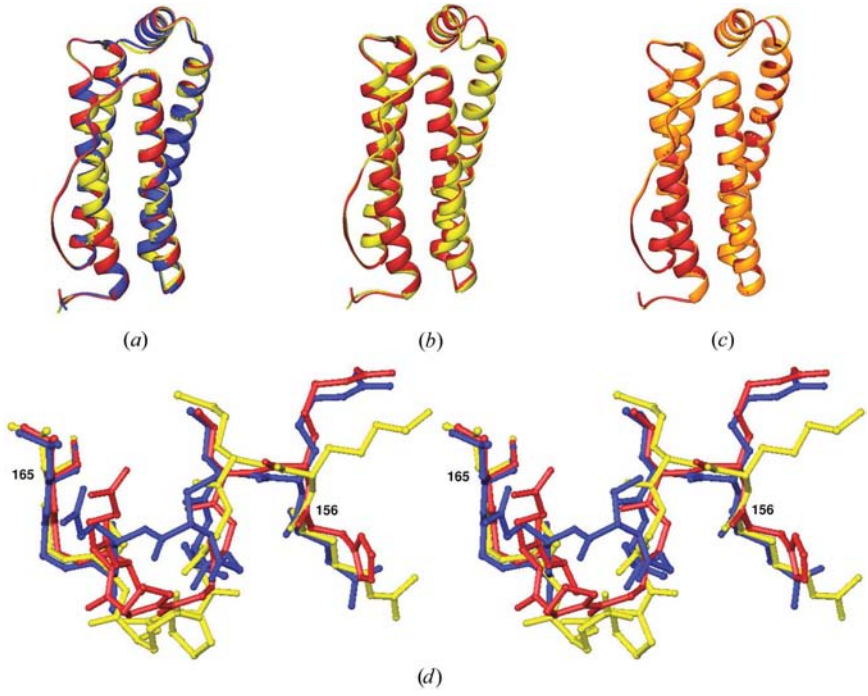

Figure 1
Structure comparisons. (*a*) Superposition of three HuLF structures. Red, *I*432 at low temperature. Yellow, *I*432 at room temperature. Blue, *R*32. (*b*) Superposition of HuLF and HuHF structures. Red, *I*432 HuLF at low temperature. Yellow, HuHF structure. (*c*) Superposition of HuLF and HoLF structures. Red, *I*432 HuLF at low temperature. Gold, HoLF structure. (*d*) Stereo diagram of *DE* loops. Red, *I*432 HuLF at low temperature. Yellow, HuHF structure. Blue, HoLF structure.

3. Results

3.1. Structural comparison of HuLF with HuHF and HoLF

The comparison between HuHF and HoLF structures has been extensively described by others (Hempstead *et al.*,

1997). We describe here the principal differences between these three structures. For ease of comparison, the amino acids in all three structures are numbered according to the HuHF sequence, starting with residue 5.

Similar to other ferritin structures, HuLF has 24 subunits, with each monomer composed of a 17-residue four-helix bundle, named *A*, *B*, *C* and *D* accordingly, and a fifth helix, *E*, linked at the C-terminal end. The Ramachandran plot showed that more than 90% residues reside within favorable regions for both structures (Table 1). The *R*32 structure has complete electron density for 174 residues. The lt-*I*432 structure contains residues 5–177, while the rt-*I*432 structure includes residues 5–175, lacking the C-terminal end. The high resolution (1.9 Å) of lt-*I*432 allowed the modeling of ten residues in alternative conformations: Ser13, Ser22, Gln29, Leu37, Arg43, Arg63, Arg79, Ser122, Arg124 and Cys130. rt-*I*432 also has six residues in alternative conformations: Ser22, His53, Arg63, Glu90, Arg124 and Cys130.

The HuLF structures of the two crystal forms are almost identical. The superposition of molecule *A* in *R*32 with lt-*I*432 gives an r.m.s. deviation of 0.37 Å for all C^{α} atoms. The superposition of rt-*I*432 with that in lt-*I*432 gives an r.m.s. deviation of 0.46 Å for all C^{α} atoms (Fig. 1*a*). Since there is little difference in main-chain conformation between these structures, we used the lt-*I*432 structure for comparison with the HuHF and HoLF structures.

Comparison of the HuLF and HoLF structures reveals a very high level of similarity, as these two proteins share 87% sequence identity. Superposition of the two structures gives an r.m.s. deviation of 0.55 Å for all C^{α} atoms. Analyses of the molecules revealed that both structures adopt essentially the same fold. The major differences reside in the *DE* turn, where helices *A*, *C* and *D* in HoLF are one amino acid longer than those in HuLF (Fig. 1*b*).

Although HuLF and HuHF only share 53% sequence identity, the two structures displayed good agreement in folding. Superposition of these two structures gives an r.m.s. deviation of 1.06 Å for all C^{α} atoms, with the largest difference being in the *DE* turn (see below). In addition, helix *A* of HuHF is longer than that of HuLF (Fig. 1*c*).

Detailed comparison of the *DE* turns (amino acids 156–165) of the three structures uncovered quite significant differences in both primary and tertiary structure. In addition to five differing amino acids in this stretch in HuLF compared with HuHF, Pro161 in HuLF adopts a *trans* conformation instead of *cis* in HuHF, which bends the loop in a different direction. HuLF and HoLF also show a high degree of sequence variation in this region. Four out of ten amino acids are different, in particular a serine in HoLF at the position of Pro161, resulting in an altered folding in this loop (Fig. 1*d*). These large deviations in the C^{α} positions of the *DE* turn do not significantly affect the overall structure of the ferritin molecules (Figs. 1*a*, 1*b* and 1*c*).

The structures of the *DE* turn in both crystal forms of HuLF are identical and both structures have very well defined electron density for this stretch of amino acids (Fig. 2). Asp162 residues from four adjacent molecules make hydrogen-bonding interactions with each other, contributing to the stability of the fourfold channel formed by *E* helices. Although this residue is not conserved in L-chain ferritins, Gln162 in HoLF also makes similar contacts. Asp162 in HuHF does not interact with neighboring molecules owing to the conformation of the *DE* turn.

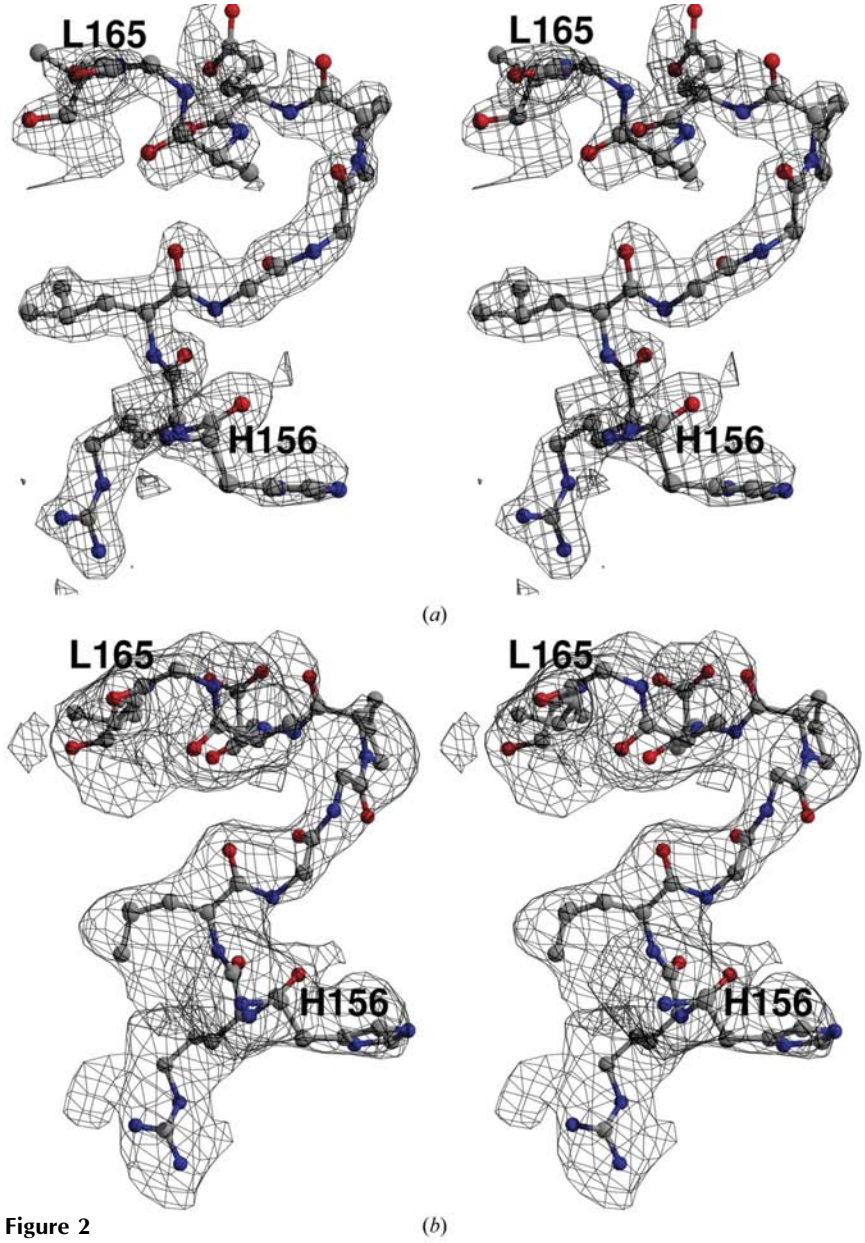

Figure 2
Stereo pictures of *DE* loops with electron-density maps. (*a*) *I*432 form. (*b*) *R*32 form.

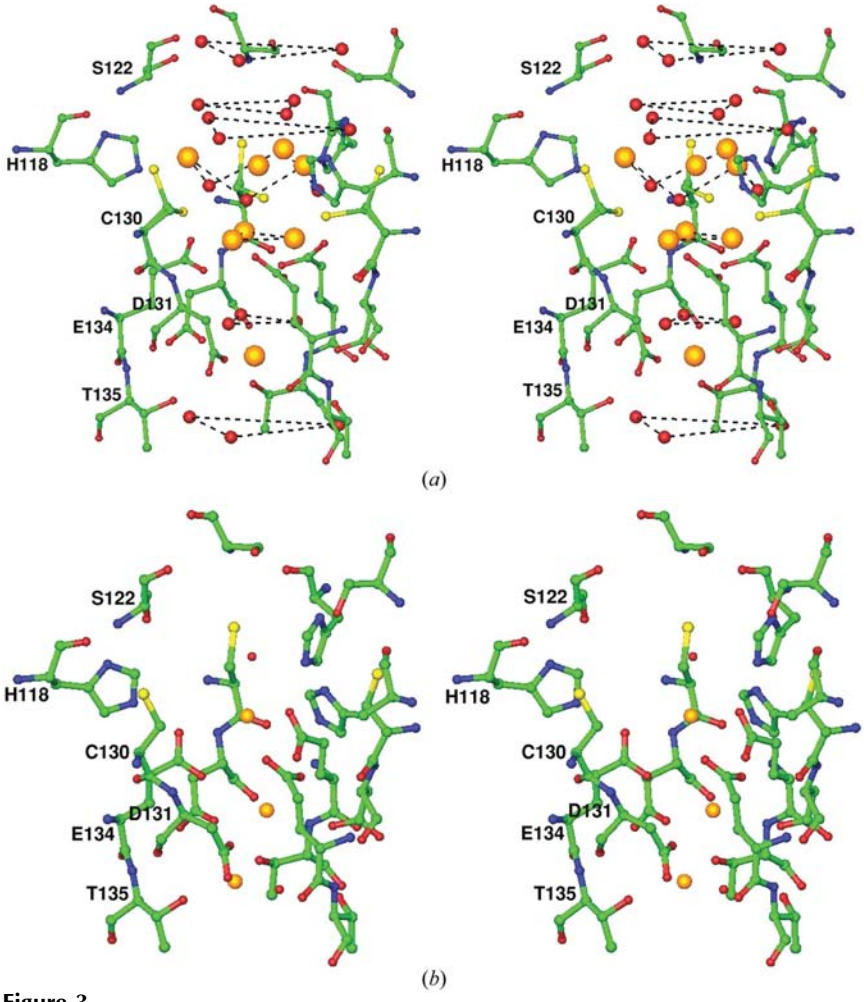

Figure 3
Stereo picture of Cd^{2+} and water molecules bound at the threefold. For simplicity, only one of the three protein molecules is labeled. Small red balls are bound water molecules and large golden balls are bound Cd^{2+} ions. (*a*) *I*432 form. (*b*) *R*32 form.

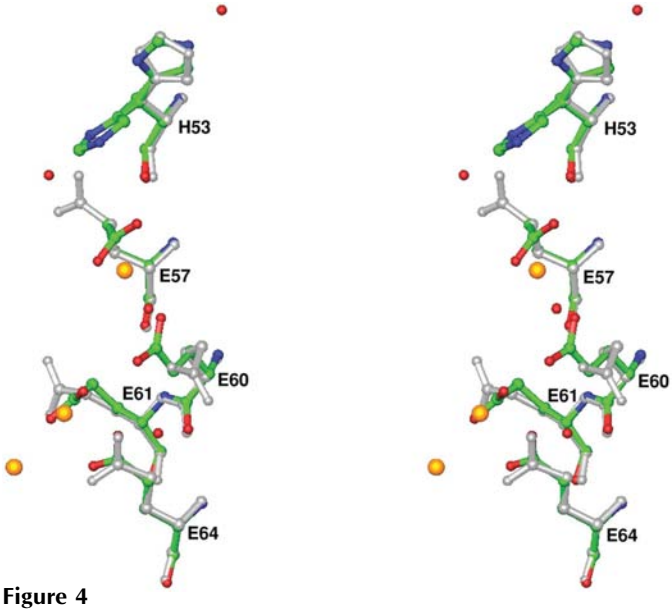

Figure 4
Comparison of the ferrihydrite nucleation centre between *I*432 and *R*32 structures. *I*432 is colored according to atom types and *R*32 is colored silver.

3.2. Intermolecular crystal contacts

The new crystal forms of HuLF exhibit very different molecular packing from HoLF and HuHF. HoLF and many other L-chain ferritins were determined in space group *F*432. The HuHF structure was determined earlier in the same *F*432 form only after genetically engineering intermolecular crystal contacts with a Lys86 to Gln mutation, creating coordination for a Ca^{2+} ion between molecules similar to that observed in HoLF (Lawson *et al.*, 1991). The amino acid at position 86 in the HuLF sequence is also a lysine as in HuHF; however, our attempts to produce useful crystals using the Lys86 to Gln mutation in HuLF were unsuccessful.

In *I*432 crystals, the closest contacts between capsids occur around the crystallographic threefold axis between molecules. The main interactions are from Ser13, Asp15 and Arg124, which interact with their twofold symmetrical partners through bound Cd^{2+} and sulfate ions (see below) owing to the existence of an intermolecular twofold axis. In the *R*32 crystal form, the closest contacts come from a region near the N-terminal portion of a monomer, along a crystallographic twofold axis.

In the *I*432 and *R*32 crystal forms reported here, there is no intermolecular (between two 24-subunit spheres) contact from Lys86. The loop enclosing Lys86 (81–90) is involved in extensive contact with the same stretch from a neighboring monomer through a well ordered water network, which contributes to the formation of the integral capsid, not the crystal lattice.

3.3. Binding of metal ions

The two crystal forms reported here were obtained in the presence of different metal ions, providing a detailed view of the threefold iron channel and the ferrihydrite nucleation centre.

The ferritin 432 capsid has two sets of pores that penetrate the capsid evelope: one set of hydrophobic pores located at the fourfold axes and the other set, hydrophilic in character, at the threefold axes. It is largely accepted that iron makes its way into the capsid *via* the hydrophilic pores located at the threefold axes. These pores are shaped like an hourglass, with His118, Ser122, Cys130, Asp131, Glu134 and Thr135 lining the inner wall. Entering the pore from the exterior surface reveals an organized network of water molecules. The upper chamber of the pore is completely filled with a quasicrystalline array of four Cd^{2+} and 12 water molecules ordered around the threefold. The structure implies a representation of an orderly path

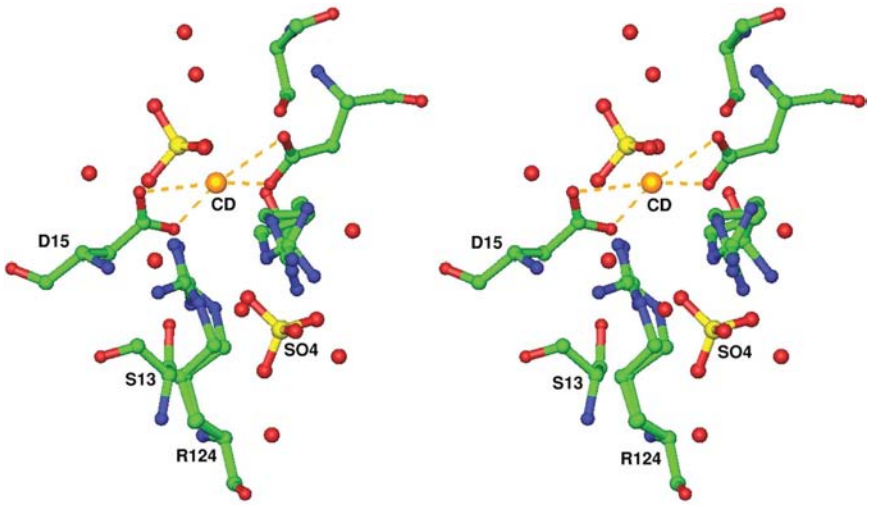

Figure 5
Stereo picture of bound Cd^{2+} and sulfate ions at the twofold axis between spheres. Only one symmetry-related partner is labeled; the small unlabeled red balls are bound water molecules.

of iron as it is shuttled into the capsid, where it is eventually oxidized at the ferroxidase centres.

The putative role of Cys130 in shuttling iron through a restricted gate has been suggested by Granier and coworkers based on the two conformations of this cysteine revealed by the high-resolution structure of recombinant light chain of horse ferritin (Granier *et al.*, 1998). This cysteine is highly conserved in heavy-chain and light-chain ferritins, except in bullfrog L-chain ferritin (Thr).

In the *R*32 structure where the crystals are grown in the presence of Cs^+ ions, only three metal ions can be identified inside the threefold channel. These three Cs^+ ions make van der Waals contacts with Asp131, Glu134 and Thr135, respectively. Here, Cys130 is only seen in one conformation, pointing away from the channel and not interacting with any water or metal ion. The exterior of the channel is open, with no ordered water structure associated with Ser122 and His114 (Fig. 3*b*). Since the concentration of Cs^+ in the crystallization condition (50 m*M*) is comparable with that of Cd^{2+} in the *I*432 form (70 m*M*), the difference in ion concentration in the channel could be attributed to the greater specificity of the channel towards divalent ions, such as iron, rendering it less capable of transporting monovalent ions such as Cs^+.

In the lt-*I*432 structure, ten Cd^{2+} ions are also identified in addition to those identified along the threefold axis. Inside the ferritin capsid, Glu57 and Glu60 coordinate a Cd^{2+}, while Glu61 and Glu64 coordinate two Cd^{2+} together. Close to the ferrihydrite nucleation centre (Granier *et al.*, 2003), His136 and Glu49 each coordinate one Cd^{2+}. Intriguingly, outside the sphere, Glu92 and Asp84 each bind one Cd^{2+}. These two residues are highly conserved among L-chain ferritins. Glu90, which is not conserved, adopts two alternative conformations that bind two Cd^{2+} with each conformation. The tenth Cd^{2+} is bound between two ferritin spheres, coordinated by Asp15 (see below).

Inside the *R*32 ferritin sphere, no strong difference density could be identified. The ferrihydrite nucleation centre has different conformations (Fig. 4). Glu57 and Glu60 point away from the centre, losing the capability to coordinate an ion. The side chains of the other pair, Glu61 and Glu64, are too far apart to coordinate ions owing to a different conformation of Glu61.

3.4. Cd^{2+} and sulfate ions between spheres

A Cd^{2+} is found on a twofold axis between two spheres in the *I*432 form. This Cd^{2+} ion is coordinated by Asp15 and its symmetry-related partner with very close contacts. The distances between Cd^{2+} and the $O^{\delta1}$ atoms of the Asp residues are 2.10 and 2.11 Å, respectively, and those between Cd^{2+} and the $O^{\delta2}$ atoms of the Asp residues are 2.66 and 2.67 Å, respectively.

Next to the Cd^{2+}, a sulfate ion is also tightly bound between the spheres. One sulfate O atom is hydrogen bonded with Ser13 O^{γ}, with a distance of 2.72 Å. Another O atom is hydrogen bonded with Arg124, which adopts two conformations, with interacting distances of 2.77 and 2.81 Å, respectively. Several water molecules also contributed to the coordination in the vicinity of this region (Fig. 5).

4. Discussion

The reported structures are the first human L-chain ferritin structures to be solved at high resolution. The crystals were obtained with the original sequence without any mutations. Although HuLF shares only 53% sequence identity with HuHF, the structures of each subunit and the overall assembly are very similar. The significant difference lies in the flexible *DE* turn, in which Asp162 from HuLF interacts with symmetrical partners to stabilize the assembly. Despite HuLF and HoLF being 87% identical in amino-acid sequence, the *DE* turns in these structures are still different. This region is highly ordered and identical in our two structure forms, eliminating differences caused by artificial crystal contacts. The interactions from the *DE* turn, which is not found in H-chain ferritins, could also account for the significantly increased stability of the L chains toward chemical or heat denaturation.

The high resolution of the lt-*I*432 form enabled detailed modeling of metal binding inside the threefold ion channel. The binding of water molecules and Cd^{2+} ions in this region allows us to speculate on the mechanism of iron uptake. The charged residues on the exterior of the channel could act as magnets to attract iron ions. Once the iron ions get into the channel, Cys130 will carry them further by swinging its side chain up and down to shovel the iron ions into the narrow gate to be coordinated by Glu134 and Asp131. After the iron ions get through the channel, they start clustering at the ferrihydrite nucleation centre composed of Glu57, Glu60, Glu61

and Glu64. The binding of ions in the *I*432 form, distinctive from that in the *R*32 form, implicates the transport specificity of ferritin molecules.

The work reported here is part of a series of studies involving ferritin as a model system in the exploratory application of microgravity for the production of large macromolecular crystals suitable for neutron diffraction analysis. Determining the hydrogen positions and ionization states for the ordered residues will be an invaluable aid in elucidating further chemistry of the iron channel, ferrihydrite nucleation and ferroxidase centres.

We are grateful to Drs Dieter Snyder and Anand Saxena at BNL Biology Department for providing us with facilities on beamline X12B and assistance during data collection. This work was supported in part by grant NAG8-1828 to DCC from the National Aeronautics and Space Administration.

References

Brünger, A. T., Adams, P. D., Clore, G. M., DeLano, W. L., Gros, P., Grosse-Kunstleve, R. W., Jiang, J.-S., Kuszewski, J., Nilges, M., Pannu, N. S., Read, R. J., Rice, L. M., Simonson, T. & Warren, G. L. (1998). *Acta Cryst.* D**54**, 905–921.

Ford, G. C., Harrison, P. M., Rice, D. W., Smith, J. M. A., Treffry, A., White, J. L. & Yariv, J. (1984). *Philos. Trans. R. Soc. Lond. B Biol. Sci.* **304**, 551–565.

Gallois, B., Langlois d'Estaintot, B., Michaux, M. A., Dautant, A., Granier, T. & Precigoux, G. (1997). *J. Biol. Inorg. Chem.* **2**, 360–367.

Granier, T., Comberton, G., Gallois, B., d'Estaintot, B. L., Dautant, A., Crichton, R. R. & Precigoux, G. (1998). *Proteins*, **31**, 477–485.

Granier, T., Langlois d'Estaintot, B., Gallois, B., Chevalier, J. M., Precigoux, G., Santambrogio, P. & Arosio, P. (2003). *J. Biol. Inorg. Chem.* **8**, 105–111.

Harrison, P. M. & Arosio, P. (1996). *Biochim. Biophys. Acta*, **1275**, 161–203.

Hempstead, P. D., Yewdall, S. J., Fernie, A. R., Lawson, D. M., Artymiuk, P. J., Rice, D. W., Ford, G. C. & Harrison, P. M. (1997). *J. Mol. Biol.* **268**, 424–448.

Laskowski, R. A., MacArthur, M. W., Moss, D. S. & Thornton, J. M. (1993). *J. Appl. Cryst.* **26**, 283–291.

Lawson, D. M., Artymiuk, P. J., Yewdall, S. J., Smith, J. M., Livingstone, J. C., Treffry, A., Luzzago, A., Levi, S., Arosio, P., Cesareni, G., Thomas, C. D., Shaw, W. V. & Harrison, P. M. (1991). *Nature (London)*, **349**, 541–544.

Sack, J. S. & Quiocho, F. A. (1997). *Methods Enzymol.* **277**, 158–173.

Theil, E. C. (1987). *Annu. Rev. Biochem.* **56**, 289–315.

Trikha, J., Theil, E. C. & Allewell, N. M. (1995). *J. Mol. Biol.* **248**, 949–967.